Rapid Communications | Editors' Suggestion

# Unexpected termination switching and polarity compensation in $LaAlO_3/SrTiO_3$ heterostructures

Guneeta Singh-Bhalla,[1,2] Pim B. Rossen,[3] Gunnar K. Pálsson,[2,4,*] Matthew Mecklenburg,[5] Thomas Orvis,[6] Sujit Das,[3] Yun-Long Tang,[3] Jaganatha S. Suresha,[7] Di Yi,[3,†] Abhigyan Dasgupta,[1] David Doenning,[8] Victor G. Ruiz,[8] Ajay K. Yadav,[3] Morgan Trassin,[3,‡] John T. Heron,[3,§] Charles S. Fadley,[2,4] Rossitza Pentcheva,[9] Jayakanth Ravichandran,[6,¶] and Ramamoorthy Ramesh[1,2,3,‖]

[1]*Department of Physics, University of California, Berkeley, California 94720, USA*
[2]*Materials Science Division, Lawrence Berkeley National Laboratory, Berkeley, California 94720, USA*
[3]*Department of Materials Science and Engineering, University of California, Berkeley, California 94720, USA*
[4]*Department of Physics, University of California, Davis, California 95616, USA*
[5]*Core Center of Excellence for Nano Imaging (CNI), University of Southern California, Los Angeles, California 90089, USA*
[6]*Mork Family Department of Chemical Engineering and Materials Science, University of Southern California, Los Angeles, California 90089, USA*
[7]*National Center for Electron Microscopy, Lawrence Berkeley National Laboratory, Berkeley, California 94720, USA*
[8]*Department of Earth and Environmental Sciences and Center of Nanoscience (CENS), University of Münich, DE-80333 Münich, Germany*
[9]*Department of Physics and Center for Nanointegration (CENIDE), University of Duisburg-Essen, 47057 Duisburg, Germany*

(Received 4 January 2018; revised manuscript received 26 August 2018; published 21 November 2018)

Polar crystals composed of charged ionic planes cannot exist in nature without acquiring surface changes to balance an ever-growing dipole. The necessary changes can manifest structurally or electronically as observed in semiconductors and ferroelectric materials through screening charges and/or domain wall formation. In the case of prototypical polar complex oxides such as the $LaAlO_3/SrTiO_3$ system the nature of screening charges for different interface terminations is not symmetric. Electron accumulation is observed near the $LaAlO_3/TiO_2$-$SrTiO_3$ interface, while the $LaAlO_3/SrO$-$SrTiO_3$ stack is insulating. Here, we observe evidence for an asymmetry in the surface chemical termination for nominally stoichiometric $LaAlO_3$ films in contact with the two different surface layers of $SrTiO_3$ crystals, $TiO_2$ and SrO. Using several element-specific probes, we find that the surface termination of $LaAlO_3$ remains $AlO_2$ irrespective of the starting termination of $SrTiO_3$ substrate surface. We use a combination of cross-plane tunneling measurements and first-principles calculations to understand the effects of this unexpected termination on band alignments and polarity compensation of $LaAlO_3/SrTiO_3$ heterostructures. An asymmetry in $LaAlO_3$ polarity compensation and resulting electronic properties will fundamentally limit atomic level control of oxide heterostructures.

DOI: 10.1103/PhysRevMaterials.2.112001

When cleaved, polar crystals composed of charged ionic planes may become highly unstable depending on the crystallographic orientation and the associated charges of the exposed surface. An electric dipole moment that is inherent to the layered structure can emerge, giving rise to a potential that diverges with thickness [1]. Such polar instabilities in nature may be compensated through complicated structural and chemical surface reconstruction processes such as rumpling of the surface atoms, adatom absorption, stoichiometric changes, or electronic processes such as screening charge accumulation [2–5]. An additional degree of complexity arises when polar crystals are directly in contact with other materials and band alignments influence the reconstruction process [4,6]. This effect has a profound influence on the electronic properties of polar compound semiconductors and ferroelectric materials. For instance, improper screening of ferroelectric polarization can have direct influence on the nature of domain structure. In the case of complex oxide heterostructures, a curious asymmetry is observed when polar $LaAlO_3$ films are grown on $SrTiO_3$ crystals with either an SrO or $TiO_2$ surface layer. An electron gas appears at the "*n*-type" $SrTiO_3$-$TiO_2/LaAlO_3$ interface for $LaAlO_3$ thicker than four to six unit cells (u.c.), but the "*p*-type" $SrTiO_3$-$SrO/LaAlO_3$ interface is insulating [7–9]. Accumulation of free charge at the *n*-type interface is thought to play a role in screening the dipole across $LaAlO_3$ [10–12]. Analogously, a dipole is also expected to form across $LaAlO_3$ for the *p*-type system requiring a positive charge at the interface for screening, but experimentally the interface is insulating [7,10]. One study suggests that localized oxygen vacancies at the *p*-type interface may screen the dipole, although the work focused on multilayers, which differ from the bilayer $SrTiO_3/LaAlO_3$

*Present address: Department of Physics and Astronomy, Uppsala University, Uppsala, 751 20, Sweden.
†Present address: Department of Applied Physics, Stanford University, Stanford, CA 94305, USA.
‡Present address: Department of Materials, ETH Zurich, Vladimir-Prelog-Weg 4, 8093 Zurich, Switzerland.
§Present address: Department of Materials Science and Engineering, University of Michigan, Ann Arbor, Michigan 48109, USA.
¶Corresponding author: jayakanr@usc.edu
‖Corresponding author: rramesh@berkeley.edu

 

heterostructure in both growth dynamics and band alignments [10]. Furthermore, two core level photoemission results show evidence of finite but opposite polar fields across $LaAlO_3$ for the *p*-type system, which are smaller than the ideal field for the *n*-type interface [13,14]. Hence the origin of the asymmetrical electric properties for the two heterostructures has heretofore remained largely unresolved. A fundamental understanding of the polarization compensation mechanisms in model oxide heterostructures such as $SrTiO_3/LaAlO_3$ is crucial for developing controlled interfaces and devices for oxide electronics [4,15,16].

Our observations for the *p*-type heterostructure reveal an unexpected chemical change on the top $LaAlO_3$ surface, which may carry implications for electronic properties of the $LaAlO_3/SrTiO_3$ system. For $LaAlO_3$ films grown on $SrTiO_3$(001) single crystals, we expect to obtain $SrTiO_3$-$TiO_2$-SrO-$TiO_2$/LaO-$AlO_2$-LaO-$AlO_2$- $\cdots$ -LaO-$AlO_2$ for the *n*-type heterostructure and $SrTiO_3$-$TiO_2$-SrO/$AlO_2$-LaO-$AlO_2$-LaO-$\cdots$ -$AlO_2$-LaO for the *p*-type structure [Fig. 1(a)]. Assuming formal valencies as labeled in Figs. 1(a) and 1(b), and using a parallel plate capacitor approximation, a net internal electric field ($\mathscr{E}$) will appear between every other layer as depicted by arrows [1,10]. Hence, a diverging dipole requiring surface reconstructions should be present for both heterostructures, albeit with opposite polarity (see red curve, Fig. 1 inset, (c), (d) for the *p*-type system, and Supplemental Material Figs. S1 and S2 for the *n*-type system [18] for simple sheet charge model and first principles calculations). In fact, theoretical calculations suggest that the polarity-induced defect mechanisms could explain the electronic properties of polar heterostructures such as the $LaAlO_3/SrTiO_3$ system [17].

In this work, we use a combination of three element-specific probes such as time-of-flight–ion scattering and recoil spectroscopy (TOF-ISARS), angle-resolved x-ray photoelectron spectroscopy (AR-XPS), and high-resolution scanning transmission electron microscopy (STEM) combined with cross-plane transport measurements and first-principles calculations to probe the surface composition and its potential effects on the polarity of $LaAlO_3$ for both heterostructures. Although formally we expect an $LaO^+$ surface layer for the *p*-type heterstructure and $AlO_2^-$ for the *n*-type heterostructure, using AR-XPS and TOF-ISARS, we measure instead an $AlO_x^-$ surface layer for both systems. STEM studies confirm the presence of atomically sharp interfaces in both the *n*-type and *p*-type heterstructures, which is an important requirement to rule out any issues due to intermixing between the layers, and further support the integrity of the conclusions drawn from the AR-XPS and TOF-ISARS studies.

The details of the film growth and characterizations, and theoretical calculations are provided in the Supplemental Materials [18]. We begin the experimental studies by confirming the $TiO_2$ and SrO surface terminations of $SrTiO_3$ (001) oriented substrates using TOF-ISARS. The TOF-ISARS [19] setup used for this study consists of angle-resolved mass spectroscopy of recoiled ions (AR-MSRI) and direct recoil spectroscopy (DRS) by Ionwerks Inc. (Houston, TX). We used AR-MSRI primarily for all the results discussed here, but we will use the terms TOF-ISARS and AR-MSRI interchangeably. Two substrates of each termination were prepared

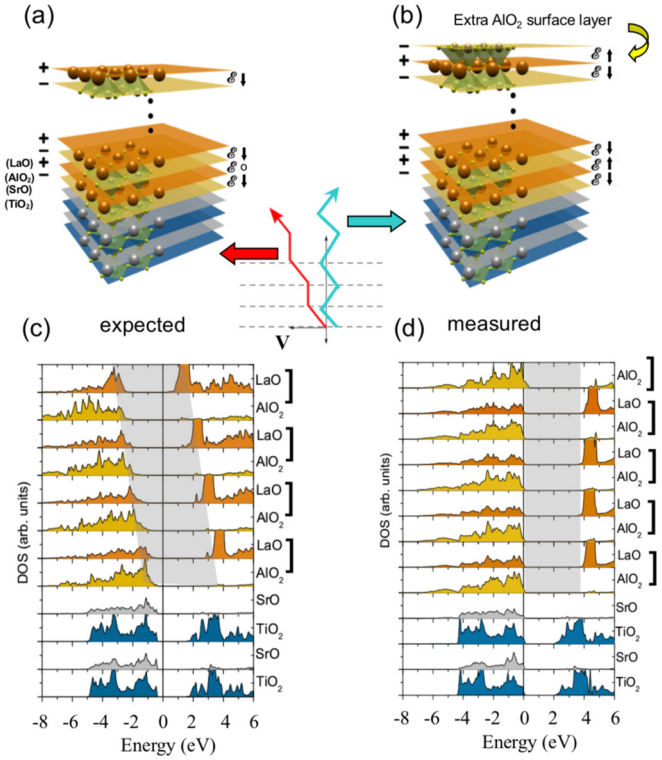


FIG. 1. A comparison of the theoretically expected and experimentally observed *p*-type $LaAlO_3/SrTiO_3$ heterostructure, both with and without an additional ionic layer that cancels $LaAlO_3$'s diverging dipole. (a) The schematic depicts the expected atomic layer stacking for a *p*-type $LaAlO_3/SrTiO_3$ heterostructure. $SrTiO_3$ terminates with SrO (gray) at the interface, in direct contact with $AlO_2^-$ (yellow). $LaAlO_3$ terminates at the $LaO^+$ (orange) surface layer. Vertical ellipses convey an arbitrary $LaAlO_3$ thickness. The net charge in the ionic limit is labeled to the left of the $LaAlO_3$ stack, while the net electric field ($\mathscr{E}$) is depicted on the right using arrows. The center inset depicts the resulting potential which grows with thickness (blue) for the expected *p*-type structure. (b) The *p*-type $LaAlO_3$ stack with an additional $AlO_x^-$ (ideally $AlO_2^-$) layer as confirmed by measurements is shown. Neighboring layers have an equal and opposite $\mathscr{E}$, resulting in no net potential (red arrow, center inset). Hence the extra surface $AlO_x^-$ layer cancels the dipole. (c) The layer-resolved density of states (LDOS) calculated using DFT are shown for a *p*-type four-u.c.-thick $LaAlO_3$ stack, as depicted in (a), with the $LaO^+$ top surface. The presence of $\mathscr{E}$ is reflected in shifts of the O $2p$ and La $4f$ bands. (d) LDOS of the same system as in (c) adding an extra $AlO_2^-$ layer diminishes $\mathscr{E}$.

using standard techniques [20–22]. Figure 2(a) shows relative intensities of the $Ti^+/Sr^+$ ratios obtained from the AR-MSRI. Single termination is revealed in the form of a clear asymmetry in the ratio of $Ti^+$ to $Sr^+$ ions at a measurement angle of 45°, along the [110] direction for the two terminations. As depicted in the inset to Fig. 2(a), at this angle the $Ti^+$ and $Sr^+$ ions shadow one another, hence only the topmost layer of $SrTiO_3$ is probed [23–25]. At 0°, the incident beam is aligned along the [100] and [010] directions equally along rows of $Sr^+$ and $Ti^+$ ions. The mixed termination of an untreated $SrTiO_3$ substrate, on the other hand, reveals nearly equivalent ratios for the $Ti^+$ and $Sr^+$ ions at 45° and 0°.

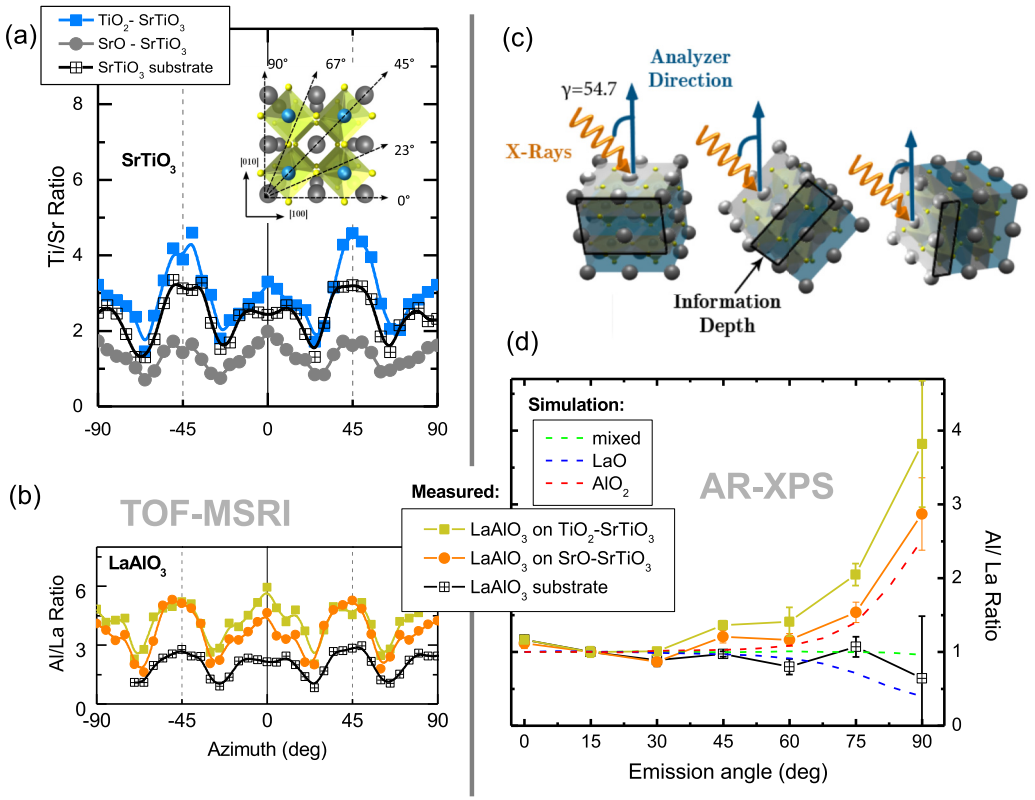


FIG. 2. TOF-ISARS and AR-XPS measurements show an $AlO_x^-$ top surface for $LaAlO_3$ in both the $n$-type and $p$-type heterostructure geometries. (a) TOF-ISARS is used to confirm the surface termination of $SrTiO_3$ substrates. $K^+$ ions impinge the surface at an angle of 15° as the sample is rotated about the azimuth ($x$ axis). The scattered and recoiled ions reflect the atomic structure and mass of the surface species. At 45° when the $A$- and $B$-site atoms shadow one another, we see an enhanced ratio of Ti/Sr at 0° for the $TiO_2$ -terminated substrates compared to the SrO-terminated substrates. (b) Using TOF-ISARS we find an $Al^+$-rich surface for $LaAlO_3$ grown on both the $TiO_2$ ($n$-type ) and SrO ($p$-type ) $SrTiO_3$ surfaces. (c) The schematic depicts our AR-XPS setup with a fixed angle $\gamma = 54.7°$ between the incoming x rays and the analyzer. The sample is rotated about an angle $\alpha$ (not shown) with respect to the analyzer. (d) AR-XPS measurements are compared to SESSA simulations for the various $LaAlO_3$ surface terminations as labeled. Clearly, $LaAlO_3$'s top surface terminates with an $AlO_x^-$ layer for both the $p$-type and $n$-type geometries, in agreement with TOF-ISARS. Additional simulations comparing the measurement results to stoichiometric changes in subsurface $LaAlO_3$ layers, as well as intermixing with the $SrTiO_3$ elemental species are also considered. The best agreements between the data and simulations are achieved by considering a stoichiometric $LaAlO_3$ layer terminated with an $AlO_x^-$ top layer.

Following $LaAlO_3$ deposition, the surface was probed *in situ* using the same technique for two of each $p$-type and $n$-type heterostructures. Figure 2(b) compares $LaAlO_3$ films grown on the two different $SrTiO_3$ terminations along with a mixed termination bulk $LaAlO_3$ crystal with (001) orientation. As noted above, we expect an $LaO^+$ surface layer for $LaAlO_3$ in the $p$-type geometry and $AlO_2^-$ for the $n$-type geometry. Instead, we find that $LaAlO_3$ in both the $n$-type and $p$-type geometries displays the same $Al^+/La^+$ ratio, indicating a surface layer rich in $Al^+$. We note a slight decrease in the $Al^+/La^+$ ratio at zero degrees, indicating a slightly $Al^+$ poor surface for the $p$-type sample, as compared to the $n$-type sample.

AR-XPS measurements [26] of $LaAlO_3$ in each heterostructure corroborate the TOF-ISARS findings, clearly revealing an $AlO_x^-$ termination for both types of interfaces. By varying the angle of electron emission, $\alpha$, relative to the analyzer [depicted in Fig. 2(c)], the mean electron escape depth, $\Lambda(\alpha) = \Lambda\cos(\alpha)$, is varied. If an element is closer to the surface, its relative intensity will be enhanced as $\alpha$ is increased. Figure 2(d) compares the measured ratio between the areas of the Al 2$s$ and La 4$d$ peaks with simulations using the commercially available SESSA (Simulation of Electron Spectra for Surface Analysis) software package, for both heterostructures as well as the mixed termination $LaAlO_3$ crystal [27,28]. The ratio increases with $\alpha$ for both heterostructures but remains roughly constant for the mixed termination substrate. This is consistent with SESSA simulations for an $AlO_2$ (red curve) and mixed $LaAlO_3$ termination (green curve), respectively. The results were reproduced for two additional copies of the samples on two different spectrometers. $LaAlO_3$ in the $n$-type geometry terminates with the expected $AlO_x^-$ surface layer. If the $p$-type $LaAlO_3$ surface were terminated with the expected $LaO^+$ layer one would instead expect a decrease in the Al 2$s$/La 4$d$ ratio with increasing $\alpha$ [Fig. 2(d), blue curve]. However, in agreement with the TOF-ISARS results, we find that just as for the $n$-type system, $LaAlO_3$ in the $p$-type system also terminates with an $AlO_x^-$ surface layer. Furthermore, we find a slightly reduced ratio of Al 2$s$/La 4$d$ ratio for the $p$-type structure than for the $n$-type structure, again in agreement with the TOF-ISARS results. The two surface probes thus reveal consistent results. In the Supplemental Material [18],

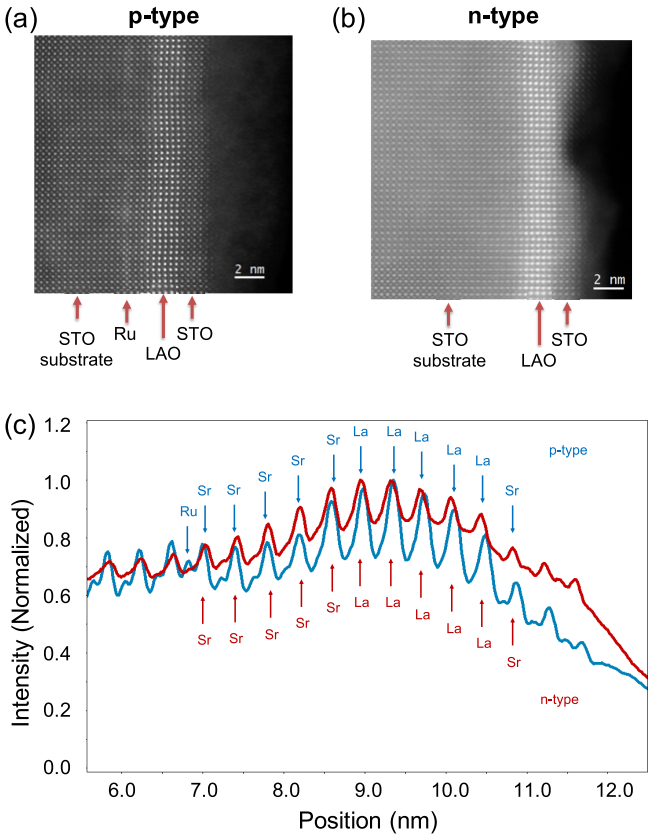


FIG. 3. ADF-STEM images show atomically sharp interfaces for both $n$-type and $p$-type heterostructures. (a),(b) Cross-sectional STEM images for five-u.c.-thick $n$-type and $p$-type heterostructures, capped with a 10-u.c.-thick $SrTiO_3$ (STO) layer are shown in the top and bottom panel, respectively. (c) ADF intensity profiles for the $p$-type (blue) and $n$-type (red) heterostructure cross sections as shown in (a) and (b). The $RuO_2$, SrO, and $LaO_2$ layers are highlighted as Ru, Sr, and La. The contrast in the intensity profiles was used to estimate the identity of each deposited u.c. type (abbreviated to the high-$Z$ component).

the measured data are further compared to SESSA simulations for a variety of scenarios including off-stoichiometric films or surface layers with $La^+/Al^+$ ratios above or below unity, as well as $Al^+$ - and $Al^+$-poor surfaces. As seen in the Supplemental Material (Fig. S3) [18], the best agreement between the SESSA simulations and measured data was achieved for a stoichiomentric $LaAlO_3$ film grown on either substrate termination of $SrTiO_3$ with a top surface of $AlO_2^-$ in both cases.

To learn about the atomic structure of the entire $SrTiO_3/LaAlO_3$ stack and allow the visualization of its layer arrangement, high-resolution STEM imaging was carried out using a FEI Titan Themis S/TEM 60–300 kV microscope. Cross-sectional STEM imaging of the layered architecture for both the $p$-type (top) and $n$-type (bottom) heterostructures is shown in Figs. 3(a) and 3(b), suggesting the presence of atomically abrupt, epitaxial interfaces between $LaAlO_3$ and $SrTiO_3$. The images were acquired along the perovskite pseudocubic direction (surface normal) and exhibit atomic columns with two distinct intensities: the La and Sr atomic columns appear brighter than the Ti and Al columns. The presence of the $RuO_2$ layer in the $p$-type heterostructure is also highlighted. Figure 3(c) shows annular dark field (ADF) intensity profiles along the line displayed in the corresponding STEM images [Fig. 3(a)]. The intensity profile clearly shows the consistent number of $LaAlO_3$ and $SrTiO_3$ layers in the $n$-type and $p$-type type heterstructures with the exception of the extra $RuO_2$ layer highlighted in the $p$-type heterostructure.

The ADF-STEM results confirm the atomically sharp interfaces in $n$-type and $p$-type heterostructures, which confirms the integrity of the conclusions drawn from TOF-ISARS and AR-XPS results for the $AlO_x^-$ surface termination for $LaAlO_3$ in both the $p$-type and $n$-type heterostructures, in addition to the $SrTiO_3$ substrate termination. In this regard, when considering formal valencies and approximating the ionic charge for each layer within $LaAlO_3$, an important consequence of the observed surface termination is the existence of a polarity built into $LaAlO_3$ for the $n$-type heterostructure [Fig. 1(a)], but ionically compensated for the $p$-type system by the extra $AlO_x^-$ layer [Fig. 1(b)]. This key difference between the dipoles across $LaAlO_3$ for the two stacking geometries can be verified using density functional theory (DFT) as shown in Figs. 1(c), 1(d), and S1. For a four-u.c.-thick $LaAlO_3$ film within the expected $p$-type geometry, Fig. 1(c) shows the presence of an internal electric field, $\mathscr{E}$, reflected in shifts of the O $2p$ and La $4f$ bands in subsequent layers to lower energies. The internal electric field is partially screened by lattice polarizations that are of opposite sign to those observed for the $n$-type $LaAlO_3/SrTiO_3$ system as shown in Fig. S2 [29,30]. Calculations for a $p$-type system where an additional $AlO_2$ layer is added on top of the four u.c. $LaAlO_3$ film are shown in Fig. 1(d). In contrast to the $LaO^+$-terminated system, the layer-resolved density of states shows that $\mathscr{E}$ is now canceled and the system is insulating except for some holes in the surface layer that are likely to be compensated by oxygen vacancies. With the presence of an additional $AlO_2^-$ layer on the $LaAlO_3$ top surface, we find that there is no measurable lattice polarization. Hence, within the DFT simulation, the extra $AlO_2^-$ layer screens the dipole for the $p$-type system.

While the mechanism for accumulating an additional $AlO_2^-$ layer is unclear and beyond the scope of the present study, we probe the influence it may have on $LaAlO_3$ polarity. A common method for measuring the electronic signatures of a built-in potential across polar dielectrics entails measuring the tunneling current density ($J$) across the dielectric layer as a function of thickness, $d$, within a parallel plate capacitor geometry, i.e., a metal-insulator-metal (MIM) tunnel junction. For a typical insulator in a MIM configuration, when a set bias voltage, $V$, is applied across the junction, $J$ decreases exponentially with increasing $d$, thus $J \propto e^{-d}$. If, however, there is a built-in potential $V_{bi}$ present across the dielectric, the applied $V$ will be offset as $V_{bi}$ grows with thickness. As the thickness of a polar dielectric such as $LaAlO_3$ varies, any unscreened potential will grow with $d$ bending the bands in the dielectric until the valence band crosses the Fermi level at a critical thickness, $d^{cr}$, and results in a sudden large increase of the overall tunneling current density, $J$. Such an increase in $J$ by orders of magnitude was previously observed at a critical thickness for $n$-type structures [11,31]. Hence, the potential across a polar dielectric can be modulated by changing $d$

to affect $V_{bi}$, or by modulating the applied bias, $V$. This phenemonon has previously been observed in wide-band-gap III-V nitrides and also ferroelectric insulators [31–33].

Such $J$ vs $d$ analysis has previously been carried out in great detail for the $n$-type $LaAlO_3/SrTiO_3$ system, in direct analogy to the wide-band-gap polar III-V nitrides [11,31]. Intriguingly, a $d_{LAO}^{cr}$ was identified at which a sudden increase in $J$ by orders of magnitude coincided with an alignment between the valence band of $LaAlO_3$ and the $SrTiO_3$ conduction band, from which a value of 80.1 meV/Å was extracted for the polar field across $LaAlO_3$ in the $n$-type $LaAlO_3/SrTiO_3$ geometry. For the $p$-type structures in the present configuration, the electrostatic arguments depicted in Fig. 1 predict no $V_{bi}$ across $LaAlO_3$, so that $J \propto e^{-d}$ as for a typical MIM junction. Hence, in stark contrast to the polarized $LaAlO_3$ in the $n$-type structure, no sudden increase in $J$ would be expected at a critical thickness for the unpolarized $LaAlO_3$ in the $p$-type structure.

In order to verify this hypothesis, we measured the tunnel current density ($J$) between $SrTiO_3$ and a Pt electrode evaporated on the $LaAlO_3$ surface [inset of Fig. 4(a)], as a function of $LaAlO_3$ thickness ($d_{LAO}$). For the present study, $J$ was measured as a function of applied bias, $V$, between the Pt electrode and 0.01 wt % $La^+$-doped $SrTiO_3$ substrates, which provide a conducting bottom electrode especially for the insulating $p$-type interface. Four tunnel junctions on each of seven $n$-type and $p$-type samples of varying thicknesses were measured. The doping level of the substrates results in a bulk carrier density below that of the induced electron gas, ensuring that an accumulation of free charge is still required to screen the $LaAlO_3$ built-in field. Figure 4(a) shows $|J|$ vs $d_{LAO}$ as measured for $V = 0.1$ V for the $p$-type heterstructures and $V = -0.1$ V for the $n$-type heterostructure. We choose the opposite polarity of $V$ for the $n$-type and $p$-type systems because a built-in field of opposite polarity would be expected for each (for electrons tunneling from the Pt electrode to the electron gas and vice versa, respectively) [11,31]. While a sudden increase of $J$, nearly seven orders of magnitude, is found at $d_{LAO}^{cr} = 20$ u.c. for the $n$-type heterostructure, as previously observed in Ref. [11], no such increase in $J$ is found for the $p$-type heterostructure. As expected, the $p$-type system behaves as a typical MIM tunnel junction, where $J \propto e^{d_{LAO}}$. Relaxation of the $LaAlO_3$ films with thickness [34] cannot alone explain the sudden increase in $J$ measured across the $n$-type heterostructure at 20 u.c. since the same would also be expected for the $p$-type heterostructure, but is not observed. We also show reciprocal space maps of the $p$-type and $n$-type heterostructures (see Supplemental Material Fig. S4 [18]) to rule out the possibility of strain relaxation and/or other spurious mechanisms causing this large, abrupt change in the tunneling current density for the $n$-type structure, but not the $p$-type structure.

The observed $|J|$ vs $d_{LAO}$ trend can be understood as follows. Figures 4(b) and 4(c) illustrate hypothetical band diagrams for two thicknesses of the $n$-type and $p$-type systems at $V = 0$. The net $V_{bi}$ for a given $LaAlO_3$ thickness, $d_{LAO}$ is the sum of net ionic potential at that thickness $V_i(d_{LAO})$, plus the potential due to the band bending resulting from work-function mismatch, $V_m$. Hence, $V_{bi} = V_i(d_{LAO}) + V_m$. While $V_m$ remains constant with thickness, $V_i(d_{LAO})$ will

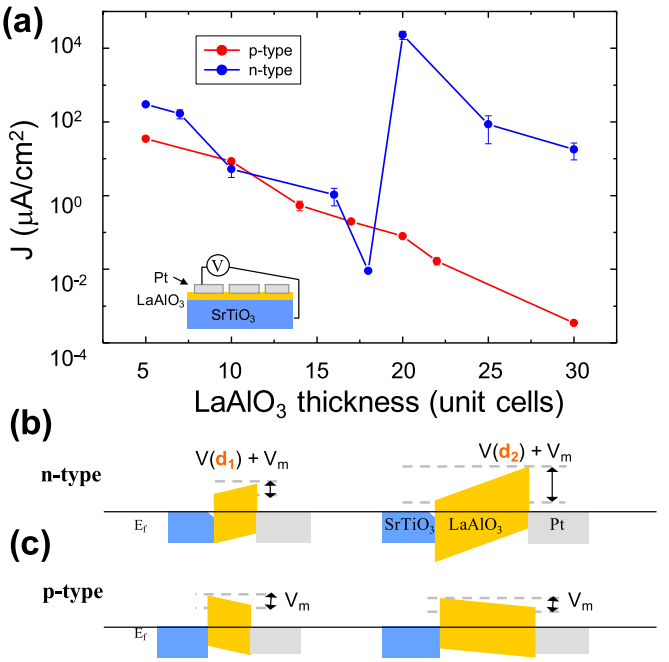


FIG. 4. Tunneling measurements reveal the presence of a dipole across $LaAlO_3$ in the $n$-type geometry but not the $p$-type geometry. (a) Room-temperature measurements of tunneling current, $J$, as a function of barrier thickness, $d_{LAO}$, across $Pt/LaAlO_3/La:SrTiO_3$ junctions is shown in logarithmc scale at $V = -0.1$ V ($n$ type) and 0.1 V ($p$ type). As expected, there is an exponential decrease in current up to $d_{LAO} = 20$ u.c. for both $p$-type and $n$-type junctions. However, a sudden increase in $J$ is observed above 20 u.c. as previously observed [11] in the presence of a dipole. $J$ across the $p$-type junction, however, continues to exponentially decrease with increasing thickness, revealing no signatures of a dipole. (b) and (c) show schematics depicting possible $n$-type and $p$-type $Pt/LaAlO_3/La:SrTiO_3$ junction band diagrams with a band misalignment potential $V_m$ that remains constant with thickness and $V(d_{LAO})$, the potential arising from an unscreened dipole that grows with thickness.

grow with thickness in the presence of a finite $LaAlO_3$ dipole until the conduction and valence bands align, giving rise to a sudden increase in $J$ [11]. Hence, in accord with previous results [11,31], the blue curve in Fig. 4(a) implies a finite $V_i(d_{LAO})$ for the $n$-type system, while the red curve implies $V_i(d_{LAO}) = 0$ for the $p$-type system, as sketched in Figs. 4(b) and 4(c). Our results imply that while a dipole can be revealed by externally applying a potential across $LaAlO_3$ that perturbs the screening charge for the $n$-type heterostructure, as previously measured [11], for the $p$-type heterostructure evidence of an analogous dipole is not detected. Hence, it is possible, as suggested by the first-principles results above, that the $AlO_x^-$ layer indeed cancels the $LaAlO_3$ polarity through an ionic (rather than electronic) reconstruction. Our observations may help explain the lack of conductivity in $SrTiO_3$ at the $p$-type interface, although further study by a variety of probes would be required for verification.

Thus, transport measurements suggest that no built-in polarity is present across $LaAlO_3$ in the $p$-type configuration with the extra $AlO_2^-$ layer. In light of the transport measurements combined with the discovery of the added $AlO_2^-$ layer,

it is tempting to speculate that the extra layer forms as a result of energetics: i.e., it could be energetically more favorable for the system to accumulate an extra $AlO_x^-$ top surface layer than to sustain a divergent dipole in the *p*-type configuration. To this end, we note that our result is in agreement with a recent photoemission study where the core level shifts for the *p*-type system did not qualitatively agree with theoretical predictions (similar to Figs. 1(a) and 1(c)), and the authors speculate that negative charge in some form must accumulate on the top surface of $LaAlO_3$ [14]. Further studies, beyond the scope of the present work, are needed to understand the origin of the $AlO_2^-$ layer and its influences on the $LaAlO_3/SrTiO_3$ system. For instance, it is possible that the additional $AlO_x^-$ layer may accumulate immediately following growth by attracting residual $Al^{3+}$ atoms from the deposition atmosphere, or among other scenarios, it is also for instance possible that $Al^{3+}$ from the bulk of the film migrates to the surface to form the extra layer following deposition. As shown in the Supplemental Material [18], AR-XPS simulations rule out the latter scenario.

In summary, we have shown compelling evidence for an unexpected top surface termination for $LaAlO_3$ grown on SrO-terminated $SrTiO_3$, using a variety of element-specific probes. Intriguingly, the system acquires an additional half unit cell. Results from cross-plane tunneling current measurements across $LaAlO_3$, and first-principles calculations suggest that in the presence of the extra $AlO_2^-$ layer, polarity across the *p*-type $LaAlO_3/SrTiO_3$ is compensated and the system is in electrostatic equilibrium. The observed asymmetry may indicate a basic limitation to bottom-up, atomic scale design of material surfaces and interfaces, especially complex oxides, which are subject to various competing degrees of freedom. For instance, we have shown that control of $LaAlO_3$'s top surface via the well-known technique of $SrTiO_3$ surface termination is nontrivial. Essentially, a single atomic layer (SrO vs $TiO_2$) can dramatically alter the way in which heterostructures balance various energy scales such as work function mismatch and built-in ionic potentials. Additional studies of polarity compensation and the critical length scales involved are needed for a variety of materials in order to develop a general understanding of the reconstruction processes and dynamics in polar heterostructures.

*Note added*. Recently, another relevant article on the layer rearrangement at the interface of $LaFeO_3/n$-$SrTiO_3$ heterostructures was brought to our attention [35]. We also note that the recent observation of electron and hole bilayer gases in $LaAlO_3/SrTiO_3$ is not in conflict with the studies reported here [36].

The authors thank D. Schlom and D. Meier for insightful discussions and review of the manuscript. Electron microscopy was performed at The Aerospace Corporation, El Segundo, CA. The AR-XPS was conducted at the Materials Science Division, Lawrence Berkeley National Laboratory. TOF-ISARS and tunneling measurements were conducted at UC Berkeley. The work was supported by the Office of Science, Basic Energy Sciences, Materials Sciences and Engineering Division of the U.S. Department of Energy under Contract No. DE-AC02-05CH11231. G.K.P. acknowledges the International Union for Vacuum Science, Technique and Applications and the Swedish Research Council for financial support, with partial support from the Army Research Office Multi-University Research Grant No. W911-NF-09-1-0398. J.R. acknowledges support from the Air Force Office of Scientific Research (AFOSR) under Grant No. FA9550-16-1-0335. R.P. and D.D. acknowledge funding by the DFG within SFB/TR80 project C03/G03 and computational time at the Leibniz Rechenzentrum, project pr87ro.

[1] P. W. Tasker, J. Phys. C: Solid State Phys. **12**, 4977 (1979).
[2] R. Hesper, L. H. Tjeng, A. Heeres, and G. A. Sawatzky, Phys. Rev. B **62**, 16046 (2000).
[3] J. Goniakowski, F. Finocchi, and C. Noguera, Rep. Prog. Phys. **71**, 016501 (2008).
[4] C. Noguera and J. Goniakowski, J. Phys.: Condens. Matter **20**, 264003 (2008).
[5] C. Noguera and J. Goniakowski, *Oxide Materials at the Two-Dimensional Limit* (Springer, Cham, 2016), pp. 201–231.
[6] X. Gu, I. S. Elfimov, and G. A. Sawatzky, arXiv:0911.4145.
[7] A. Ohtomo and H. Y. Hwang, Nature (London) **427**, 423 (2004).
[8] S. Thiel, G. Hammerl, A. Schmehl, C. W. Schneider, and J. Mannhart, Science **313**, 1942 (2006).
[9] M. Huijben, G. Rijnders, D. H. A. Blank, S. Bals, S. Van Aert, J. Verbeeck, G. Van Tendeloo, A. Brinkman, and H. Hilgenkamp, Nat. Mater. **5**, 556 (2006).
[10] N. Nakagawa, H. Y. Hwang, and D. A. Muller, Nat. Mater. **5**, 204 (2006).
[11] G. Singh-Bhalla, C. Bell, J. Ravichandran, W. Siemons, Y. Hikita, S. Salahuddin, A. F. Hebard, H. Y. Hwang, and R. Ramesh, Nat. Phys. **7**, 80 (2011).
[12] Y. Xie, Y. Hikita, C. Bell, and H. Y. Hwang, Nat. Commun. **2**, 494 (2011).
[13] Y. Segal, J. H. Ngai, J. W. Reiner, F. J. Walker, and C. H. Ahn, Phys. Rev. B **80**, 241107 (2009).
[14] M. Takizawa, S. Tsuda, T. Susaki, H. Y. Hwang, and A. Fujimori, Phys. Rev. B **84**, 245124 (2011).
[15] S. Gariglio, M. Gabay, and J.-M. Triscone, APL Mater. **4**, 060701 (2016).
[16] M. Lorenz, M. R. Rao, T. Venkatesan, E. Fortunato, P. Barquinha, R. Branquinho, D. Salgueiro, R. Martins, E. Carlos, A. Liu *et al.*, J. Phys. D **49**, 433001 (2016).
[17] L. Yu and A. Zunger, Nat. Commun. **5**, 5118 (2014).
[18] See Supplemental Material at http://link.aps.org/supplemental/10.1103/PhysRevMaterials.2.112001 for sample fabrication and characterization details.
[19] J. W. Rabalais, *Principles and Applications of Ion Scattering Spectrometry* (Wiley, New York, 2003).
[20] M. Kawasaki, K. Takahashi, T. Maeda, R. Tsuchiya, M. Shinohara, O. Ishiyama, T. Yonezawa, M. Yoshimoto, and H. Koinuma, Science **266**, 1540 (1994).
[21] G. Rijnders, D. H. A. Blank, J. Choi, and C.-B. Eom, Appl. Phys. Lett. **84**, 505 (2004).

[22] P. Yu, W. Luo, D. Yi, J. X. Zhang, M. D. Rossell, C.-H. Yang, L. You, G. Singh-Bhalla, S. Y. Yang, Q. He *et al.*, Proc. Natl. Acad. Sci. USA **109**, 9710 (2012).

[23] A. Gozar, G. Logvenov, V. Y. Butko, and I. Bozovic, Phys. Rev. B **75**, 201402 (2007).

[24] J. E. Kleibeuker, G. Koster, W. Siemons, D. Dubbink, B. Kuiper, J. L. Blok, C.-H. Yang, J. Ravichandran, R. Ramesh, J. E. ten Elshof *et al.*, Adv. Funct. Mater. **20**, 3490 (2010).

[25] A. Biswas, P. B. Rossen, C.-H. Yang, W. Siemons, M.-H. Jung, I. K. Yang, R. Ramesh, and Y. H. Jeong, Appl. Phys. Lett. **98**, 051904 (2011).

[26] C. Baeumer, C. Xu, F. Gunkel, N. Raab, R. A. Heinen, A. Koehl, and R. Dittmann, Sci. Rep. **5**, 11829 (2015).

[27] C. P. W. Smekal and W. S. M. Werner, Surf. Interface Anal. **37**, 1059 (2005).

[28] W. S. M. Werner and W. Smekal, NIST Database for the Simulation of Electron Spectra for Surface Analysis (SESSA) Version 1.3, Standard Reference Data Program Database 100, http://www.nist.gov/ts/msd/srd/nist100.cfm (2010).

[29] R. Pentcheva and W. E. Pickett, Phys. Rev. B **78**, 205106 (2008).

[30] R. Pentcheva and W. E. Pickett, Phys. Rev. Lett. **102**, 107602 (2009).

[31] J. Simon, Z. Zhang, K. Goodman, H. Xing, T. Kosel, P. Fay, and D. Jena, Phys. Rev. Lett. **103**, 026801 (2009).

[32] A. Bykhovski, B. Gelmont, M. Shur, and A. Khan, J. Appl. Phys. **77**, 1616 (1995).

[33] C. Wetzel, T. Takeuchi, H. Amano, and I. Akasaki, Phys. Rev. B **61**, 2159 (2000).

[34] C. Cancellieri, D. Fontaine, S. Gariglio, N. Reyren, A. D. Caviglia, A. Fête, S. J. Leake, S. A. Pauli, P. R. Willmott, M. Stengel *et al.*, Phys. Rev. Lett. **107**, 056102 (2011).

[35] S. R. Spurgeon, P. V. Sushko, S. A. Chambers, and R. B. Comes, Phys. Rev. Mater. **1**, 063401 (2017).

[36] H. Lee, N. Campbell, J. Lee, T. Asel, T. Paudel, H. Zhou, J. Lee, B. Noesges, J. Seo, B. Park *et al.*, Nat. Mater. **17**, 231 (2018).